UC 413

LBL-29566
Preprint

Lawrence Berkeley Laboratory

UNIVERSITY OF CALIFORNIA

Physics Division

Submitted to Nuclear Instruments and Methods
in Physics Research A

Ion Motion in a Small Low Energy Cyclotron

K.J. Bertsche

September 1990

For Reference

Not to be taken from this room

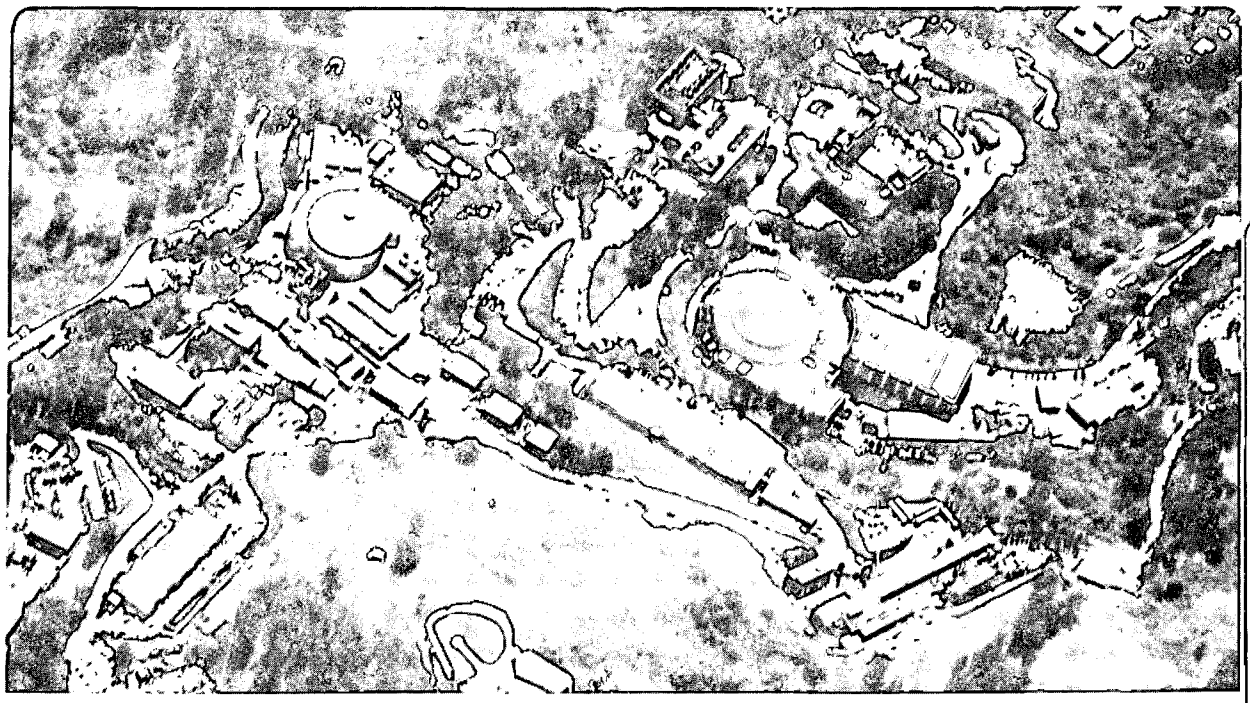

Prepared for the U.S. Department of Energy under Contract Number DE-AC03-76SF00098.

LBL-29566
Copy 1
Bldg. 50 Library.

DISCLAIMER

This document was prepared as an account of work sponsored by the United States Government. While this document is believed to contain correct information, neither the United States Government nor any agency thereof, nor the Regents of the University of California, nor any of their employees, makes any warranty, express or implied, or assumes any legal responsibility for the accuracy, completeness, or usefulness of any information, apparatus, product, or process disclosed, or represents that its use would not infringe privately owned rights. Reference herein to any specific commercial product, process, or service by its trade name, trademark, manufacturer, or otherwise, does not necessarily constitute or imply its endorsement, recommendation, or favoring by the United States Government or any agency thereof, or the Regents of the University of California. The views and opinions of authors expressed herein do not necessarily state or reflect those of the United States Government or any agency thereof or the Regents of the University of California.

ION MOTION IN A SMALL LOW ENERGY CYCLOTRON

Kirk J. Bertsche
Lawrence Berkeley Laboratory
University of California
Berkeley, CA 94720

ABSTRACT

A small cyclotron (the "cyclotrino") was proposed for direct detection of radiocarbon in 1980 and has now detected radiocarbon at natural abundance. High resolution and background rejection are achieved in this cyclotron by acceleration of negative ions through many turns while operating at a high harmonic.

This paper details the analysis of ion motion in a small flat-field, electrostatically-focused cyclotron. Included are discussions of beam acceptance, axial and radial beam stability, and a detailed analysis of phase bunching and its effect on mass resolution.

This work has been supported by the U.S. Department of Energy under contract DE-AC03-76SF00098.

1. INTRODUCTION

The small cyclotron project was begun at Berkeley in 1981 [1] in response to the increasing demand and high cost of existing accelerator mass spectrometry (AMS) techniques. The basic idea was to combine the excellent properties of a cyclotron used as a mass spectrometer with the capabilities of negative ion sources to reject unwanted backgrounds such as ^{14}N [2,3].

A small cyclotron (the "cyclotrino") was built at Berkeley to test these concepts [4-7]. This cyclotron incorporated a miniature Cs sputter negative ion source at the center of the cyclotron, injecting negatively-charged carbon ions at about 3 keV. Extraction energy was about 40keV at about a 10.5 cm radius. The cyclotron was operated at the 11th to 15th harmonic to obtain the necessary resolution and relied solely on electrostatic focusing for ion confinement. It was found that such a device did indeed produce the necessary resolution for detection of ^{14}C, although radiocarbon at natural abundance could not be detected because of the low output of the internal ion source which was used.

The cyclotron was rebuilt to provide for a high-current external ion source [8-10]. This cyclotron is very similar in design to the earlier machine, with the addition of an external ion source and injection beamline, and is shown in Fig. 1. Radiocarbon has been detected at natural abundance in this device [10-12].

Our initial work has emphasized ^{14}C. Measurements of other radioisotopes, such as ^{26}Al, ^{10}Be and ^{3}He are also possibilities with the cyclotrino but have not been pursued.

2. DESIGN CONSIDERATIONS

The cyclotron which we have studied is a two-dee cyclotron, each dee subtending 180°. Thus the electric fields are imposed at two positions in the particle's orbit, displaced 180° from each other. In such a design the electric fields may be driven at the cyclotron frequency or at any odd harmonic of the cyclotron frequency. Harmonic operation will improve the resolution of a cyclotron used as a mass spectrometer, since mass resolution is roughly proportional to the product of the number of turns and the harmonic [4,6].

We use sinusoidal excitation, though with the relatively low RF voltages occurring in a cyclotron used as a low-energy mass spectrometer, non-sinusoidal excitation could be considered and has been suggested by other researchers [13].

The cyclotrino was designed specifically for ^{14}C. It operates with negative ions to avoid interference from ^{14}N. With ^{14}N eliminated, the nearest interfering mass is the molecular ion ^{13}CH, which is heavier than ^{14}C by a part in 1800. This sets the minimum resolution requirements. The necessary resolution is obtained by operating at a high harmonic (11th to 15th) of the fundamental cyclotron frequency and by using a very flat magnetic field, which causes orbits to be isochronous and hence allows ions to make many turns (50 to 100) in the cyclotron.

For operation with ^{14}C, we use a magnetic field of about 1 Tesla. Beam is injected at an energy of 5 keV with a 2.8 cm radius and extracted at about 40keV with a 10 cm radius. Ions must gain about 260 eV in the first two gap crossings for about half of them to clear an electrostatic deflection channel in the center of the cyclotron (see section 3).

This cyclotron is typically operated with a harmonic of 11 to 15 and a peak dee voltage of 300 to 400 volts. The cyclotron frequency is about 1 MHz with a magnetic field of about 1 Tesla, so the dees must be driven at 11 to 15 MHz at 600 to 800 volts peak-to-peak.

Beam from an external, high current negative ion source is captured by an electrostatic einzel lens, pre-seperated by a Wien filter, and focused by a series of electrostatic quadrupole lenses. It is then injected radially into the cyclotron using electrostatic deflectors and an electrostatic mirror [14]. The system is shown schematically in Fig. 2.

3. ENERGY GAIN

Calculation of the electric field distribution across the dee gap allows energy gain per turn, turn separation, and number of turns to be calculated. The field distribution may be analytically solved using certain approximations.

Firstly, the electrostatic approximation may be employed. In this cyclotron, the time taken for the electric field to propagate in the gap region is so small as to be negligible,

i.e. $b/c << 1/\omega_{RF}$ where b is the dee height, c is the speed of light, and ω_{RF} is the RF frequency. Thus, the electric potential distribution between the dees is approximately that for an electrostatic problem; the solution is simply the electrostatic potential with a time-varying amplitude.

Secondly, it may be assumed that the gap between the dees is infinitesimal. While this assumption is not necessary (solutions for the case of a finite gap have been presented by Murray and Ratner [15] and Reiser [16]), it simplifies the computations greatly and is a good approximation for this cyclotron. The dees are not excited at extremely high voltages, so it has been possible to space them very close together. (The gap is 1 to 2 mm, while the height is 8 mm.) The assumption of an infinitesimal gap will only cause errors for particles traveling very close to the dees; the field near the median plane will be relatively unaffected by this approximation.

With these approximations, an analytical expression for the electric potential in the gap region may be obtained by conformal mapping:

$$\Phi(y,z) = V\left[1 - \frac{1}{\pi}\tan^{-1}\left(\frac{\cos\frac{\pi z}{b}}{\sinh\frac{\pi y}{b}}\right)\right] \tag{3.1}$$

The resulting electric fields are:

$$E_y = -\frac{V}{b}\left(\frac{\cos\left(\frac{\pi z}{b}\right)\cosh\left(\frac{\pi y}{b}\right)}{\cos^2\left(\frac{\pi z}{b}\right) + \sinh^2\left(\frac{\pi y}{b}\right)}\right) \tag{3.2}$$

$$E_z = -\frac{V}{b}\left(\frac{\sin\left(\frac{\pi z}{b}\right)\sinh\left(\frac{\pi y}{b}\right)}{\cos^2\left(\frac{\pi z}{b}\right) + \sinh^2\left(\frac{\pi y}{b}\right)}\right) \tag{3.3}$$

where a sinusoidal excitation is assumed:

$$\begin{aligned} V &= V_m\cos(H\omega t + \phi) \\ &= V_m\cos\left(\frac{Hy}{r} + \phi\right), \text{ for } Hy << r \end{aligned} \tag{3.4}$$

and where variables are defined as:

y = distance from gap plane (in direction of ion motion)
z = distance from median plane
b = dee height (distance between top and bottom surfaces)
V = instantaneous voltage across gap (dee voltage)
V_m = peak dee voltage
H = harmonic number = ω_{RF}/ω
ω = cyclotron frequency = qB/m
ω_{RF} = RF oscillator frequency
q = ion charge
B = magnetic field strength
m = ion mass
E_y = electric field component in y direction
E_z = electric field component in z direction
ϕ = RF phase at which ion crosses dee gap
r = cyclotron radius = v/ω

The electric field is shown schematically in Figure 3.

Knowing the field distribution in the gap region, the change in kinetic energy due to a gap crossing may be easily approximated:

$$\delta T = \int F_y dy \cong \int_{-\infty}^{\infty} qE_y dy \tag{3.5}$$

where T = ion energy and the integral extending to infinity is based on the assumption that $b << r$. This integral is difficult to solve in general, but if one assumes that $\delta T << T$ (a good approximation in our case), the cyclotron radius (which appears in trigonometric arguments in the expressions for electric field) may be assumed constant across the gap. The integral may be solved by writing the denominator as a difference of squares, expanding with partial fractions and refering to integral tables [17 §3.983 #1]:

$$\delta T \cong -qV_m \cos\phi \left[\frac{\cosh \frac{Hz}{r}}{\cosh \frac{Hb}{2r}} \right] \tag{3.6}$$

The bracketed quantity is a transit-time factor [4, 6, 18 §7-10]; it tends to reduce the energy gain for ions which traverse the gap slowly compared to the period of the sinusoidal excitation of the dees.

For a negatively-charged ion (as is used in this machine) energy gain is provided only for ϕ in the first or fourth quadrant. In the second and third quadrants ions will lose energy.

From (3.6) it is simple to calculate the change in radius per gap crossing:

$$\begin{aligned}\delta r &\cong \frac{r\delta T}{2T} \\ &\cong \frac{-qV_m \cos\phi}{mr\omega^2}\left[\frac{\cosh\frac{Hz}{r}}{\cosh\frac{Hb}{2r}}\right] \\ &\cong \frac{r(\delta T)_{\max}\cos\phi}{2T}\left[\frac{\cosh\frac{Hz}{r}}{\cosh\frac{Hb}{2r}}\right] \qquad (3.7)\end{aligned}$$

where $\delta T_{\max}$ = maximum possible energy gain per turn = $-qV_m$ (negative ions are assumed). Since there are two accelerating gaps per orbit, the radial separation of orbits is twice this quantity.

The increase in radius given by the first two gap crossings must be sufficient for the ions to clear the inner deflector after the first orbit. The beam width at the position of this deflector, which is 90° from the dee gap, is a minimum and is about 2 mm. Thus, a 2 mm increase (corresponding to a 520 eV increase for a 5000 eV beam) will allow all ions to clear, while a 1 mm increase (corresponding to a 260 eV increase) will allow about half to clear. We have found that about 300 to 400 V peak voltage is necessary to clear most of the ions when running at the 11th to 15th harmonic.

The minimum number of turns may be calculated from the fact that there is a maximum energy available at each gap crossing. Thus:

$$N_{\text{turns}} \geq \frac{T_f - T_0}{2(\delta T)_{\max}}$$
$$\geq \frac{T_0}{2(\delta T)_{\max}}\left(\frac{r_f^{\,2}}{r_0^{\,2}} - 1\right) \tag{3.8}$$

where T_0 = initial ion energy, T_f = extraction energy, r_0 = initial cyclotron radius and r_f = cyclotron radius at extraction.

A more exact computation of the number of turns may be obtained with a computer program which was written to simulate ion motion in the cyclotron. This program follows the approach of Cohen [19] and Welch [4] in that the changes in energy, axial velocity and ion phase are calculated and assumed to occur instantaneously at each gap crossing. The program allows input of arbitrary ion characteristics (axial position, axial velocity and ion phase with respect to the RF waveform) and cyclotron characteristics (RF voltage, harmonic and frequency offset). An ion can be followed through the cyclotron to see the effects of different conditions.

For this cyclotron, operating at the 11th harmonic with 300 V peak, one would expect at least 50 turns based on (3.8). The actual number of turns is shown in Fig. 4 as a function of input parameters. It is seen that ions entering with 0° phase require 50 turns if they enter near the dees, since they gain the maximum energy at each gap crossing. They require more turns if they enter near the center of the dee gap because of the transit time effect. For ions which enter with 45° phase, still more turns are required, the exact number depending on axial position and angle.

4. STABILITY

In traditional (non-sectored) cyclotrons, orbit stability is dependant primarily on the magnetic field index of the machine [18 ch. 2]. The magnetic field is given a radial gradient; the field index is defined as the ratio of the fractional change in B to the fractional change in radius. In the cyclotrino it has been necessary to keep the field index as close to zero as possible to retain orbit isochronicity. Isochronous orbits are necessary if particles are to be retained for a large number of turns, which in turn is necessary for high resolution. Thus, orbit stability mechanisms in the cyclotrino are somewhat more subtle than in traditional designs.

4.1 Axial Stability

Axial stability is provided in this machine by electrostatic focusing. Sector focusing could have been used to provide focusing while retaining orbit isochronicity, but was judged more complex than necessary for this machine.

Electrostatic focusing arises from the fact that the electric field varies in both space and time. The axial impulse which an ion receives at a gap crossing may be approximated by:

$$\begin{aligned} \delta p_z &\cong \int_{t=-\infty}^{t=\infty} qE_z\,dt \\ &\cong q\int_{y=-\infty}^{y=\infty} \frac{E_z(y)}{v_y(y)}\,dy \end{aligned} \tag{4.1}$$

where, again, the approximation has been made that $b << r$. Again, it is beneficial to assume that $\delta T << T$. This simplifies trigonometric arguments as before, and also allows $v(y)$ to be approximated as constant and pulled out of the integral. The integral may be solved similarly to the integral for energy gain discussed above, using the appropriate integral tables [17 §3.984 #1]; alternatively, these two integrals (3.5 and 4.1) may be solved simultaneously by contour integration [20]:

$$\delta p_z \cong \frac{qV_m \sin\phi}{v}\left[\frac{\sinh\frac{Hz}{r}}{\cosh\frac{Hb}{2r}}\right] \tag{4.2}$$

For ϕ in the first or second quadrant a negative ion experiences a restoring force toward the median plane. These particles are focused axially, while those with ϕ in the third or fourth quadrant experience axial defocusing and are quickly lost. Thus only ions with ϕ in the first quadrant will experience simultaneous axial focusing and energy gain; only these ions will have a chance to be successfully extracted from the cyclotron.

Equation (4.2) represents the axial momentum kick provided to an ion at each gap crossing. It is obviously nonlinear in z, but for small z may be linearized:

$$\delta p_z \cong \frac{qV_m H \sin\phi}{vr \cosh\frac{Hb}{2r}} z \tag{4.3}$$

These discrete momentum changes may be approximated as a continuous momentum change, due to an equivalent force of:

$$F_{z\,\mathrm{equiv}} = \frac{\delta p_z}{\delta t} = \frac{\omega}{\pi}\delta p_z$$

The equation of axial motion is:

$$m\frac{d^2 z}{dt^2} = F_{z\,\mathrm{equiv}}$$

This differential equation may be solved for the frequency of axial oscillations, which is:

$$\omega_z = \sqrt{\frac{-qV_m H \sin\phi}{\pi m r^2 \cosh\frac{Hb}{2r}}} \tag{4.4}$$

The axial betatron frequency for ions near the cyclotron median plane is defined as:

$$\nu_z \equiv \frac{\omega_z}{\omega} = \sqrt{\frac{(\delta T)_{\max}}{T}\frac{H\sin\phi}{\pi\cosh\frac{Hb}{2r}}} \tag{4.5}$$

In this cyclotron, ions start with 5 keV energy and 3.8 cm cyclotron radius, exiting with about 35 keV energy at a 10 cm radius. The dee height is 0.8 cm. Operating at the 15th harmonic with 400 V peak RF voltage, we find that the axial betatron frequency ν_z is $0.39\sqrt{\sin\phi}$ initially and is $0.21\sqrt{\sin\phi}$ at extraction. Thus, the potential resonance at $\nu_z = 0.50$ due to mechanical imperfections is avoided [18 ch. 5]; other potential resonances at 0.33, 0.25 and 0.20 are either mild enough or are traversed so rapidly that they do not cause problems. There are no coupled resonances to radial or phase motion in this machine since, as we will show, the radial betatron frequency is 1.0 and there are no phase oscillations.

The frequency of these small axial oscillations will not remain constant throughout the acceleration process since T and r will change. Hence the amplitude of axial oscillations will not remain constant, either. The WKB approximation may be used to determine the approximate variation in amplitude of these oscillations. Following the analysis of Livingood [18 §2-9], one finds that the amplitude is proportional to $\nu_z^{-1/2}$. For a given ion, then, the amplitude of axial oscillations is proportional to:

$$\sqrt[4]{\frac{r^2 \cosh \frac{Hb}{2r}}{\sin \phi}} \tag{4.6}$$

Trajectories of ions may be studied with the computer simulation mentioned in section 3. The trajectory of a typical ion is shown in Fig. 5, illustrating axial oscillations and amplitude variations.

4.2 Radial Stability

In a uniform magnetic field, a perturbed ion will undergo radial oscillations about the unperturbed trajectory with a frequency equal to the cyclotron frequency; thus the radial betatron frequency $\nu_r = 1$. This is a potential problem, since coupling to mechanical perturbations can lead to radial instabilities. Radial motion must be analyzed in more detail to determine stability.

Radial motion can be analyzed conveniently by describing the location of the center of an ion's orbit [21]. When not in the dee gap, the orbit center is fixed and the ion describes circular motion about this point with a radius determined by ion energy. When traversing a dee gap, an ion gains energy and the center of its orbit shifts.

As an ion gains energy, the center of its orbit moves in alternate directions at each gap crossing, appearing to hop back and forth along the dee gap. The distance of each hop decreases in magnitude as the ion approaches extraction radius. For an ion whose center lies on the dee gap, the magnitude of each of these hops may be expressed as:

$$\delta x = \frac{r}{\sqrt{T_0}} \delta\left(\sqrt{T}\right) \approx \frac{r_0^2}{2T_0} \frac{\delta T}{r} \tag{4.7}$$

The distances of these hops may be summed to find the net offset of orbit centers at extraction radius due to the acceleration process. For $\delta T << T_0 << T_f$ this sum converges to a total shift of half of the initial hop:

$$\Delta x_{\text{acc}} \approx \frac{1}{2}(\delta x)_0 \tag{4.8}$$

It is important to examine the effect of perturbing the initial orbit center position from its assumed initial position on the dee gap. There are two dimensions to be considered. If the perturbation is along the dee gap by an amount Δx_0, all of the succeeding orbit centers will be offset the same amount and the final position will simply be perturbed by a distance $\Delta x = \Delta x_0$. Thus a neutral stability exists with respect to displacements along the dee gap.

However, if the perturbation is orthogonal to this, by a distance Δy_0 away from the dee gap, there is a coupling to other dimensions. The ion will reach the gap at a different time, hence at a different RF phase:

$$\Delta\phi = \frac{H\Delta y_0}{r_0}$$

If y is positive as shown in Fig. 6, the phase shift is also positive and the ion arrives later. At the next gap the ion will arrive early by the same amount. Since the energy gained at each gap crossing depends on phase, the energy gains will be unbalanced and the hops along the dee gap will be unequal. The ion's orbit center will drift in the x dimension while it maintains a constant offset $\Delta y = \Delta y_0$ from the dee gap.

The total offset Δx_{off} due to an offset Δy_0 from the dee gap may be easily approximated for a simplified case. If it is assumed that $\Delta y_0 << r/H$, ϕ constant (no phase bunching—discussed in the next section), and no transit time effect, the δx shifts experienced at each gap crossing may be summed to find:

$$\Delta x_{\text{off}} \approx \frac{H\Delta y_0}{4}\tan\phi \ln\frac{T_f}{T_0} \tag{4.9}$$

Thus ions will drift in the x dimension as shown in Fig. 6. For typical operating parameters of $T_0 = 5$ keV, $T_f = 35$ keV, $H = 15$, and assuming that $\phi \approx 30°$, one finds the drift $\Delta x_{\text{off}} \approx 4\ \Delta y_0$.

We see that the radial betatron frequency of unity gives rise to instability with respect to perturbation of initial ion positions. However, this instability is not very severe and its effects can be controlled by controlling the initial locii of orbit centers.

4.3 Phase Stability

Phase stability relies on a change in the time required to make one orbit. If orbits are truly isochronous, ion phase will be invariant. One may think that a flat field cyclotron such as this would be truly isochronous and would thus have no coupling of orbit time to phase of gap crossing, resulting in neutral phase stability for all ion phases. Such is not the case. In a flat-field machine such as the one considered here, there is a coupling of orbit time to phase of gap crossing resulting in phase bunching [22-24]. A flat field implies that the cyclotron frequency is constant, thus the total integrated angle subtended per unit time is a constant as well. Interestingly, the angle subtended by an ion in crossing the dee gap is not necessarily constant; it depends on the spatial details of energy gain and is a function of particle phase.

The region of energy gain is not infinitesimally thin but is extended in space due to fringing of the electric field in the gap. To see how this gives rise to phase shifts, one may imagine that the energy gain occurs at two planes physically separated from the dee gap by a fixed distance. It can be seen by graphical construction (Fig. 7) that if more energy gain occurs at the second plane the total subtended angle in traversing a half-orbit is greater than 180°, more time is taken and the particle phase is retarded. If more energy gain occurs on entering the dee gap, the total subtended angle for a half-orbit is less than 180° and particle phase is advanced.

Consider operation in the first quadrant of the RF cosine wave, which is necessary for simultaneous energy gain and axial focusing. A particle arriving at the waveform peak receives nearly equal energy gains on both sides of the dee gap, thus no phase shift. A particle arriving later gets more energy gain on entering the gap region than on exiting since the cosine waveform has decreased in magnitude by the time the ion exits, thus advancing its phase. It is seen that particle phase tends to be bunched toward the peak of the RF waveform.

In a real cyclotron, the energy gain does not only occur at two planes, but is distributed across the gap with a distribution which depends on a particle's axial position and velocity. The phase change due to a single gap crossing may be calculated by

integrating the angle subtended as an ion crosses the gap region and subtracting the total angle which would have been subtended if the energy gain had all occurred at an infinitesimal-width gap. Thus:

$$\delta\phi_{ion} \cong \int_{\text{gap}} \frac{dy}{r} - \left(\frac{1}{r_0} \int_{\text{first half gap}} dy + \frac{1}{r_f} \int_{\text{second half gap}} dy \right) \tag{4.10}$$

Assuming that $\delta T << T$, and that $b << r$ (the distance over which the electric field extends is on the order of b), the phase change experienced in a single gap crossing may be reduced to [10 Appendix B]:

$$\begin{aligned} \delta\phi &\cong \frac{H}{2rT} \int_{y=-\infty}^{y=\infty} y\, dT \cong \frac{H}{2rT} \int_{-\infty}^{\infty} y F_y(y) dy \\ &\cong \frac{qH}{2rT} \int_{-\infty}^{\infty} y E_y(y) dy \end{aligned} \tag{4.11}$$

where ϕ_{ion} = ion phase and ϕ = RF phase = (H)(ion phase).

This phase shift has been expressed in terms of RF phase (ϕ), which is greater than ion phase (ϕ_{ion}) by a factor of H. This allows for operation at a harmonic of the cyclotron frequency. The integral may be solved in a similar manner to the previous integrals for energy gain and axial momentum gain [10 Appendix B]:

$$\delta\phi \cong \frac{qV_m Hb}{4rT} \sin\phi \left(\frac{\cosh\left(\frac{Hz}{r}\right)\sinh\left(\frac{Hb}{2r}\right) + \frac{2z}{b}\sinh\left(\frac{Hz}{r}\right)\cosh\left(\frac{Hb}{2r}\right)}{\cosh^2\left(\frac{Hb}{2r}\right)} \right) \tag{4.12}$$

In deriving this expression it has been assumed that $\delta T << T$ and $b << r$, and that the gap between dees is infinitesimal. The total phase shift of an ion at extraction radius may be estimated with some additional approximations. If it is assumed that the ions remain near the median plane (z small), (4.12) may be approximated as:

$$\delta\phi \cong \frac{qV_m Hb}{4rT}\sin\phi\left(\frac{\sinh\left(\frac{Hb}{2r}\right)}{\cosh^2\left(\frac{Hb}{2r}\right)}\right)$$

$$\cong \frac{-\delta T_{\max}}{T}\frac{Hb}{4r}\sin\phi\left(\frac{\sinh\left(\frac{Hb}{2r}\right)}{\cosh^2\left(\frac{Hb}{2r}\right)}\right) \tag{4.13}$$

If the additional assumptions are made that the total phase shift is small ($\phi \cong$ constant) and that many turns are made in the cyclotron, the phase change $\Delta\phi_{\text{cyc}}$ as an ion traverses the cyclotron, which is the summation of the individual phase shifts $\delta\phi_{\text{RF}}$ at each gap crossing, may be approximated by an integral, which may then be simplified using (3.7) and (4.13):

$$\Delta\phi_{\text{cyc}} \cong \int \delta\phi = \int \frac{\delta\phi}{\delta r}dr \cong -\frac{Hb}{2}\tan(\phi)\int_{r_0}^{r_f}\frac{1}{\rho^2}\tanh\left(\frac{Hb}{2\rho}\right)d\rho$$

$$\cong -\tan(\phi)\ln\left(\frac{\cosh\left(\frac{Hb}{2r_0}\right)}{\cosh\left(\frac{Hb}{2r_f}\right)}\right) \tag{4.14}$$

It is apparent that the phase ϕ will not be constant as an ion traverses the cyclotron. This phase shifting may be partially compensated by offsetting the RF frequency slightly, giving an additional, constant phase shift at each gap crossing.

Suppose the RF frequency is offset slightly so that an ion of the desired species, making its first gap crossing at RF phase ϕ_s, also makes its final gap crossing at phase ϕ_s. Then:

$$\Delta\phi_{\text{RF}} = -\Delta\phi_{\text{cyc}}$$

where:

$$\Delta\phi_{\text{RF}} \propto N_c \propto \frac{1}{\delta r} \propto \frac{1}{\cos(\phi)}$$

and:

$$\Delta\phi_{\text{cyc}} \propto \tan(\phi)$$

Consider an ion beginning with phase $\phi_s + \Delta\phi_{\text{in}}$. Its final phase will be offset from ϕ_s by an amount $\Delta\phi_{\text{out}}$. In general, $\Delta\phi_{\text{out}}$ will differ from $\Delta\phi_{\text{in}}$, implying a spreading or bunching of ion phases. A phase compression factor α_{phase} can be defined:

$$\begin{aligned}\alpha_{\text{phase}} &\equiv \frac{\Delta\phi_{\text{out}}}{\Delta\phi_{\text{in}}} \\ &= \frac{d}{d\phi}\left(\phi_s + \Delta\phi_{\text{in}} + \Delta\phi_{\text{RF}} + \Delta\phi_{\text{cyc}}\right) \\ &= 1 - \ln\left(\frac{\cosh\left(\frac{Hb}{2r_0}\right)}{\cosh\left(\frac{Hb}{2r_f}\right)}\right)\end{aligned} \tag{4.15}$$

Computer calculations of phase as a function of radius for paraxial ions are shown in Figs 8a-d. In Fig. 8a, the phase bunching for the 15th harmonic and 400 V peak RF voltage is seen. The effect of offsetting the RF frequency slightly is shown in Fig. 8b. Performance at the 31st harmonic is shown in Fig. 8c,d. It is obvious that the phase bunching increases as the harmonic is raised.

The approximation given above (4.15) is in good agreement with computer calculations for low H (below about 9) in the cyclotrino. For H=15, the agreement with computer calculations is poor (Fig. 8b), while for H=31 the agreement is very poor (Fig. 8d), with α_{phase} becoming negative as calculated from (4.15), which is physically unreasonable. These disagreements seem to arise because of the approximation $\phi\equiv$constant, used in deriving (4.15). Negative values may be avoided by approximating α_{phase} as:

$$\alpha_{\text{phase}} \equiv \frac{1}{1 + \ln\left(\cosh\left(\frac{Hb}{2r_0}\right) \Big/ \cosh\left(\frac{Hb}{2r_f}\right)\right)} \tag{4.16}$$

which has the same asymptotic behavior as (4.15) for low H, but which cannot become negative as H increases. This gives good agreement with computer simulations for $H\leq 15$ in the cyclotrino, but is in error by about a factor of two at H=31.

The phase grouping effect tends to reduce the resolution of the cyclotron, as noted by Chen, Gao and Li [24]. In fact, since the phase compression (4.15,16) is independent of RF voltage (in the approximation that $\phi \equiv$constant) and since the compression increases as the harmonic is increased (as seen in (4.15,16) and Fig. 8), one may think that the resolution cannot be significantly increased by increasing the harmonic or lowering the RF voltage. This is not the case, however. Increasing the harmonic or reducing the voltage will increase the number of turns an ion makes in the cyclotron; thus the average phase shift per turn tends to be reduced and the mass resolution tends to be increased.

The mass resolution may be approximated by computer simulations of an off-mass ion which enters on-axis at 0° phase (a lower limit on the ion phases which can be focused), with the ion's mass adjusted so that it drifts in phase to exit at 60° phase (an approximate upper limit on ion phases which can successfully exit the extraction channel). This gives rise to the family of curves shown in Fig. 9 for this cyclotron. It is obvious that the resolution is approximately proportional to H/V. In fact, as the harmonic is increased, resolution increases *faster* than does the harmonic, especially for high harmonics. (*Doubling* the harmonic from 15th to 31st *triples* the resolution).

It would appear from Fig. 9 that operation at 15th harmonic and 400 V peak is not quite adequate for detection of ^{14}C, with a resolution of about 1600. However, we have found that it gives more than enough resolution to separate ^{14}C from ^{13}CH. The approximate curves in Fig. 9 understate the actual resolution because a perfectly uniform magnetic field has been assumed in the analysis. In practice, the field strength drops very slightly at larger radii, causing additional phase retardation. This tends to increase the resolution and reduce the transmission beyond what would be expected with a perfectly flat field.

5. ACCEPTANCE

The acceptance of the cyclotron can be described in terms of a 5-dimensional phase space. The components are axial position, axial velocity (or angle), radial position, radial velocity (or angle), and ion phase with respect to the RF waveform.

The cyclotron acceptance must be matched to the ion source emittance to avoid losing beam. Extrapolating from estimates of the source emittance at 20 keV, it was

estimated that about 80% of the source output should fall within 40π mm-mrad at 5 keV. This estimate of 40π mm-mrad was used for most emittance and acceptance calculations.

Radial acceptance properties may be calculated from the equations for radial motion (section 4.2). It is desired to minimize the spread of orbit centers at extraction radius. For a fixed emittance, the minimum spread of orbit centers along the dee gap may be obtained by allowing the orbit centers to "walk" a distance Δx_{off} (4.9) about equal to the initial spread in centers, Δx_0. Thus, at H = 15, the orbit centers should preferably lie in an ellipse with $\Delta x_0 \approx 4\ \Delta y_0$. Since the harmonic is variable and the cyclotrino will not always be operated at the 15th, a 6:1 ratio was decided upon. The focusing elements were designed to place orbit centers in an elliptical region along the dee gap with a semi-major axis of 3 mm and a semi-minor axis of 0.5 mm. With an injection radius of 3.8 cm, this encloses the desired emittance area of 40π mm-mrad.

Axial acceptance was determined with the computer simulation of cyclotron performance mentioned earlier. Since axial properties are coupled to ion phase, the results may be expressed as a family of axial phase plots, parametrized by ion phase (Fig. 10a-d). A beam of 40π mm-mrad may be focused to a phase space ellipse at the dee gap with semi-axes of 2 mm and 20 mrad, matching the cyclotron's axial acceptance almost exactly.

In Fig. 10a, the axial acceptance for 11th harmonic and 300 V peak is shown. Offsetting the frequency slightly, so that ions which enter with a 30° phase lag also exit with a 30° phase lag, improves the acceptance slightly (Fig. 10b). When losses due to first turn clearance (assuming 1 mm clearance, which is necessary for about half of the ions to clear) are included (Fig. 10c), it is seen that many ions are lost when operating with a 300 V peak RF voltage. Operation with 400 V peak and 15th harmonic (Fig 10d) results in about the same resolution as 300 V peak and 11th harmonic, but gives lower loss due to the higher voltage. It was found experimentally that increasing the RF voltage from 300 to 400 volts approximately doubled the transmission through the cyclotron.

These axial acceptance plots are in general agreement with those published earlier [4,6]. However, these newer simulations indicate that the acceptance for this new system is not quite so symmetric and encloses a somewhat smaller area. This is probably due to a higher ion injection energy and to the inclusion of phase bunching in the computer simulations.

Useful phase acceptance is estimated to be about 45°, based on Fig. 10a-d. If ion phase is less than about 15°, the axial acceptance shrinks dramatically due to insufficient axial focusing. If ion phase exceeds about 60°, not enough energy is gained to clear the inner deflector on the first turn.

6. CONCLUSIONS

Ion motion in a small, low energy, flat field cyclotron has been analyzed in detail. Approximate analytic expressions have been presented for energy gain, electrostatic focusing, and phase bunching. Computer simulations of acceptance, number of turns, and mass resolution have been presented as well.

It has been shown that such a cyclotron can provide the necessary resolution for detecting ^{14}C, with good phase space matching to physically-realizable ion beams. This has been experimentally verified [10-12]. It is also seen that the resolution of the cyclotrino may be increased beyond that necessary for ^{14}C, suggesting that other isotopes may be detected as well [10-12].

I wish to thank Chandu Karadi and Gabriel Paulson for assistance in computer simulations, and Dave Clark and Jim Welch for helpful discussions. This work has been supported by the U.S. Department of Energy under contract DE-AC03-76SF00098.

REFERENCES

[1] R.A. Muller, P.P. Tans, T.S. Mast and J.J. Welch, in *Proceedings of the Symposium on Accelerator Mass Spectrometry, Argonne National Laboratory, May 11-13, 1981,* Argonne National Laboratory Report ANL/PHY-81-1 (1981) 342.

[2] D.E. Nelson, R.G. Korteling and W.R. Stott, Science 198 (1977) 507.

[3] C.L. Bennett, R.P. Beukens, M.R. Clover, H.E. Gove, R.B. Liebert, A.E. Litherland, K.H. Purser and W.E. Sondheim, Science 198 (1977) 508.

[4] J.J. Welch, PhD dissertation, Lawrence Berkeley Laboratory Report LBL-21255 (1984).

[5] J.J. Welch, K.J. Bertsche, P.G. Friedman, D.E. Morris, R.A. Muller, and P.P. Tans, Nucl. Instr. & Meth. B5 (1984) 230.

[6] J.J. Welch, K.J. Bertsche, P.G. Friedman, D.E. Morris, R.A. Muller, and P.P. Tans, Nucl. Instr. & Meth. B18 (1987) 202.

[7] J.J. Welch, K.J. Bertsche, P.G. Friedman, D.E. Morris, and R.A. Muller, in *UC Accelerator Mass Spectrometry I; Proceedings of the First University of California Conference on Accelerator Mass Spectrometry, University of California, Irvine, Feb. 15, 1986,* edited by J.E. Ericson and R.E. Taylor (Institute of Geophysical and Planetary Physics, University of California, Lawrence Livermore National Laboratory, 1989) CONF-8602126.

[8] K.J. Bertsche, P.G. Friedman, D.E. Morris, R.A. Muller, and J.J. Welch, Nucl. Instr. & Meth. B29 (1987) 105.

[9] K.J. Bertsche, P.G. Friedman, R.A. Muller, and J.J. Welch, Lawrence Berkeley Laboratory Report LBL-25450 (1988).

[10] K.J. Bertsche, PhD dissertation, Lawrence Berkeley Laboratory Report LBL-28106 (1989).

[11] K.J. Bertsche, C.A. Karadi, R.A. Muller, and G.C. Paulson, to be published in Nucl. Instr. & Meth. (1990); also published as Lawrence Berkeley Laboratory Report LBL-29556 (1990).

[12] K.J. Bertsche, C.A. Karadi, and R.A. Muller, submitted to Nucl. Instr. & Meth.; also published as Lawrence Berkeley Laboratory Report LBL-29567 (1990).

[13] M. Chen, D. Li, W. Gao, X. Zhang and R. Zhou, Nucl. Instr. & Meth. A278 (1989) 409.

[14] D.E. Morris, Nucl. Instr. & Meth. A248 (1986) 297.

[15] R.L. Murray and L.T. Ratner, J. Appl. Phys. 24 (1953) 67.

[16] M. Reiser, J. Appl. Phys. 42 (1971) 4128.

[17] I.S. Gradshteyn and I.M. Ryzhik, *Table of Integrals, Series, and Products*, corrected and enlarged ed. (Academic Press, London, 1980).

[18] J.J. Livingood, *Cyclic Particle Accelerators* (Van Nostrand, Princeton, 1961).

[19] B.L. Cohen, Rev. Sci. Instr. 24 (1953) 589.

[20] C.D. Jeffries, Phys. Rev. 81 (1951) 1040.

[21] Lj.S. Milinković, K.M. Subotić and E. Fabrici, Nucl. Instr. & Meth. A273 (1988) 87.

[22] B.L. Cohen, Handbuch der Physik 44 (1959) 105.

[23] M. Chen, D. Li, W. Gao and S. Xu, in *Proceedings of the 11th International Conference on Cyclotrons and their Applications* (Tokyo, 1987).

[24] M. Chen, W. Gao and D. Li, Nucl. Instr. & Meth. A278 (1989) 402.

2. FIGURES

Figure 1 External view of the cyclotrino. The ion source is enclosed in the cage on the left. The author is adjusting the dee probe. (CBB 874-3258)

Figure 2 Cyclotron system schematic, showing injection beamline. The einzel lens and first quadrupole focus beam onto the Wien filter object slit. The Wien filter pre-separates beam and provides monitoring of ion source output. The four remaining quadrupoles focus beam into the cyclotron. (XBL 874-1819)

Figure 3 Electric field across dee gap. Electrostatic focusing is discussed in section 4.1. (XBL 8410-8761, from Welch, 1984a)

Figure 4 Computer simulation of number of turns as a function of initial ion position, for ion phases of 0 and 45°. Initial ion angle (axial velocity) has been swept over the useful range. Operation is at the 11th harmonic with 300V peak RF. (XBL 8911-4176)

Figure 5 Simulated axial position of a typical ion as it traverses the cyclotron, showing axial oscillations. Operation is at the 11th harmonic with 300 V peak RF. (XBL 8911-4220)

Figure 6 Loci of orbit centers, showing radial perturbations to ion trajectories. Initial distribution of orbit centers is shown in (*a*), leading to the final distribution in (*b*). The distribution is shifted according to (4.8) and is distorted according to (4.9). (XBL 8911-4172)

Figure 7 Origin of phase bunching in the small cyclotron. In (*a*), ions experience more energy gain upon exiting dee gap than upon entering; total angle ($\theta_1 + \theta_2$) subtended in a half-orbit is greater than 180° and ion phase is retarded. In (*b*), more energy is gained upon entering the dee gap; total subtended angle is less than 180° and ion phase is advanced. (XBL 8911-4173)

Figure 8a Phase evolution of paraxial ions, with cyclotron operating at the 15th harmonic and 400 V peak. Ions are started at 3.8 cm with initial phases at multiples of 15°. (XBL 8911-4208)

Figure 8b Phase evolution of paraxial ions, with cyclotron operating at the 31st harmonic and 400 V peak. (XBL 8911-4212)

Figure 8c Phase evolution of paraxial ions, with cyclotron operating at the 15th harmonic and 400 V peak, with RF frequency offset slightly so that ions entering with 30° phase also exit with 30° phase. (XBL 8911-4209)

Figure 8d Phase evolution of paraxial ions, with cyclotron operating at the 31st harmonic and 400 V peak, with RF frequency offset slightly so that ions entering with 30° phase also exit with 30° phase. (XBL 8911-4213)

Figure 9 Approximate resolution of cyclotron in the presence of phase bunching. These curves are a result of computer simulations of paraxial ions, with ion masses offset to allow a 60° phase lag. (XBL 8911-4263)

Figure 10a Axial acceptance of cyclotron at 11th harmonic and 300 V peak, parametrized by ion phase. (XBL 8911-4177)

Figure 10b Axial acceptance of cyclotron at 11th harmonic and 300 V peak, with RF frequency offset for 30° ions. (XBL 8911-4178)

Figure 10c Axial acceptance of cyclotron at 11th harmonic and 300 V peak for 45° ions, including the effect of losses due to first turn clearance. (XBL 8911-4179)

Figure 10d Axial acceptance of cyclotron at 15th harmonic and 400 V peak, parametrized by ion phase. (XBL 8911-4180)

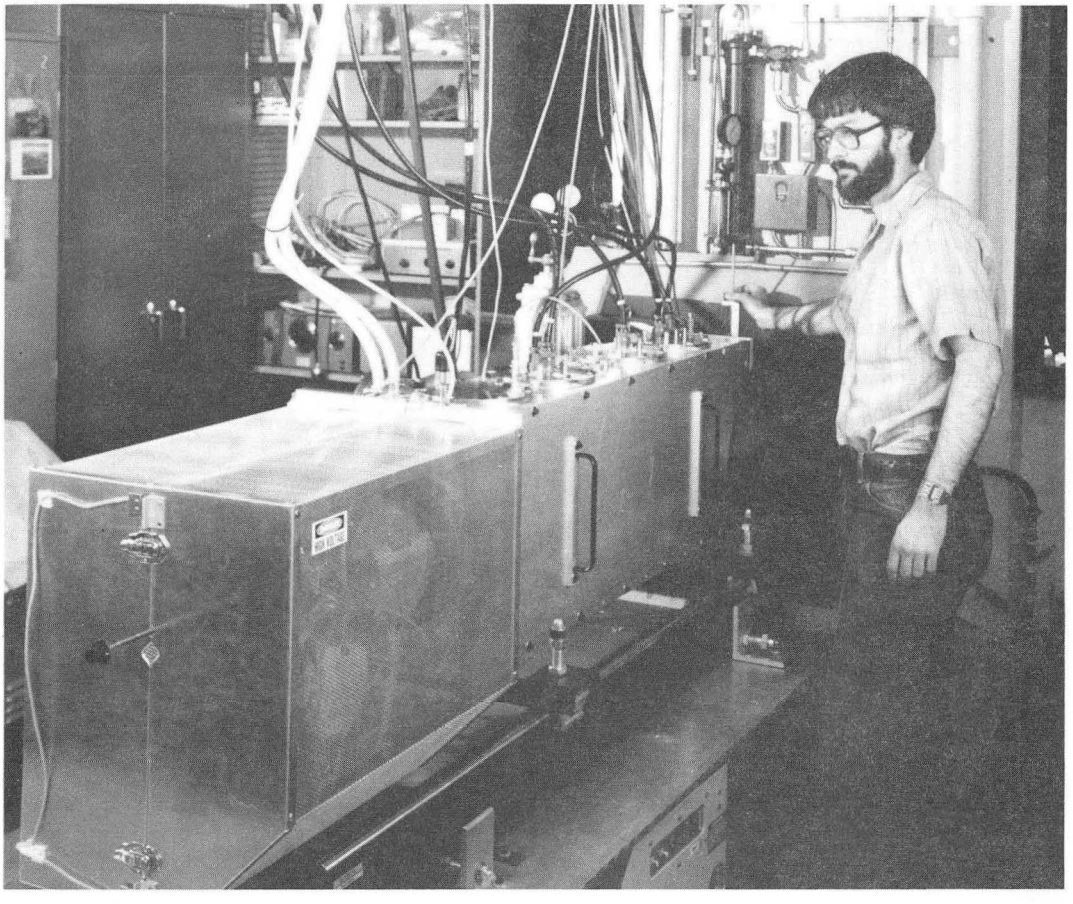

CBB 874-3258

Figure 1

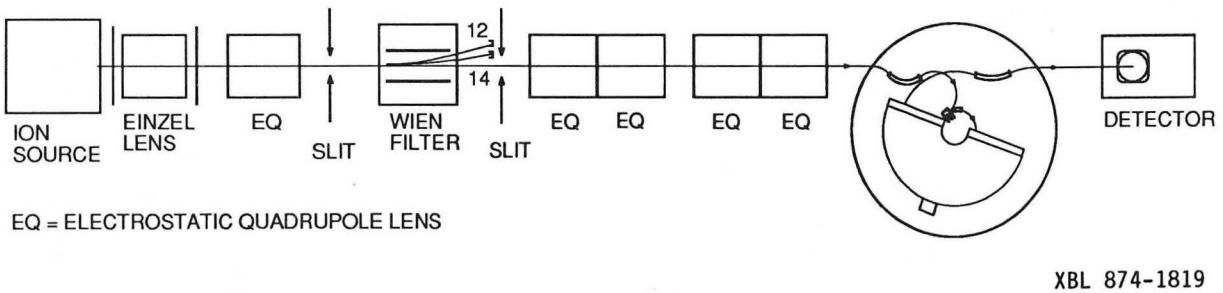
12
14
ION SOURCE
EINZEL LENS
EQ
SLIT
WIEN FILTER
SLIT
EQ
EQ
EQ
EQ
DETECTOR
EQ = ELECTROSTATIC QUADRUPOLE LENS
XBL 874-1819

Figure 2

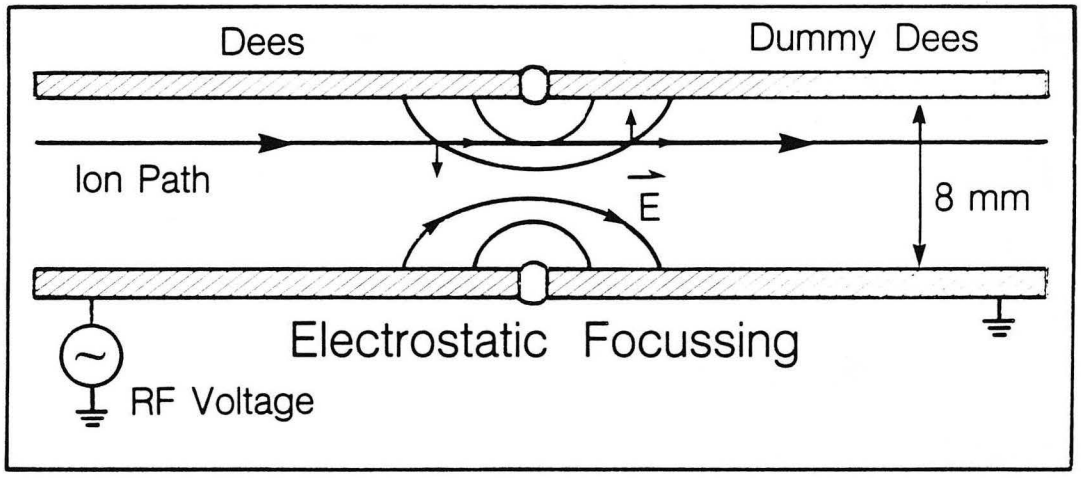

XBL 8410-8761

Figure 3

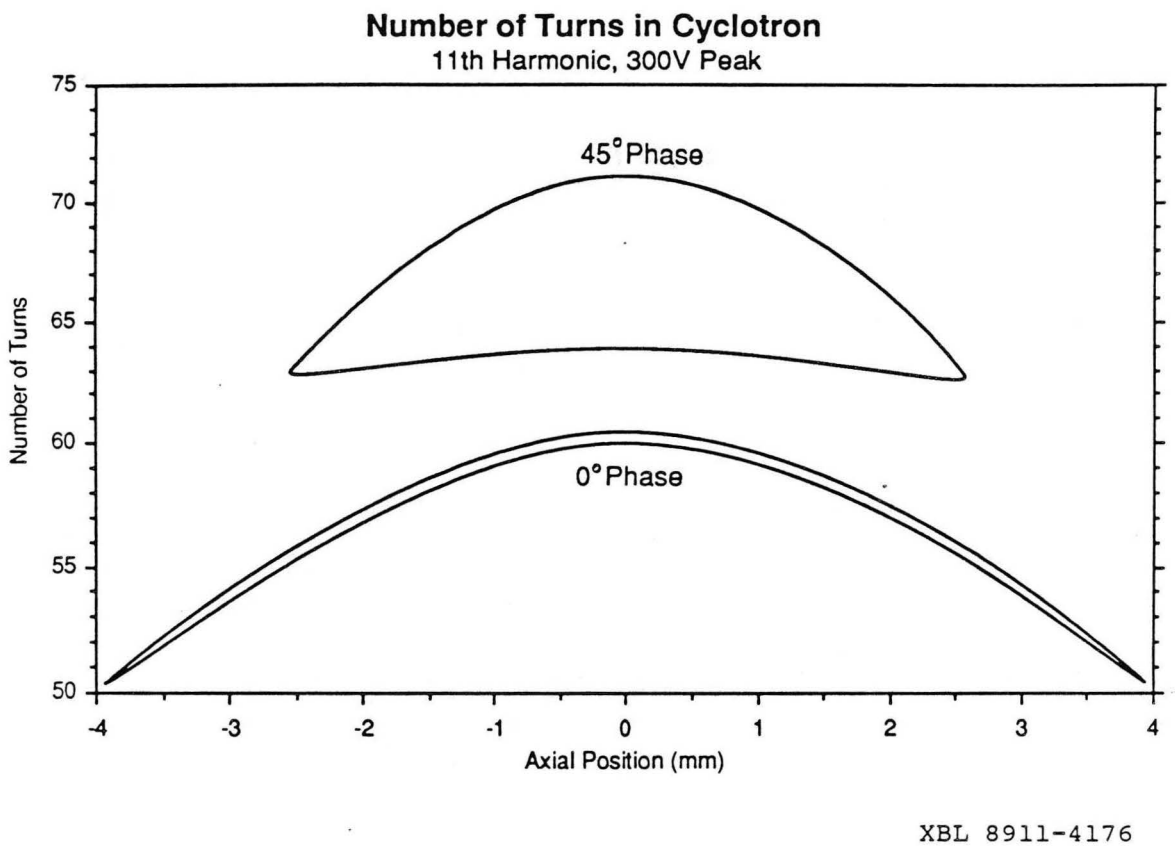
Number of Turns in Cyclotron
11th Harmonic, 300V Peak
45° Phase
0° Phase
Number of Turns
75
70
65
60
55
50
-4
-3
-2
-1
0
1
2
3
4
Axial Position (mm)
XBL 8911-4176

Figure 4

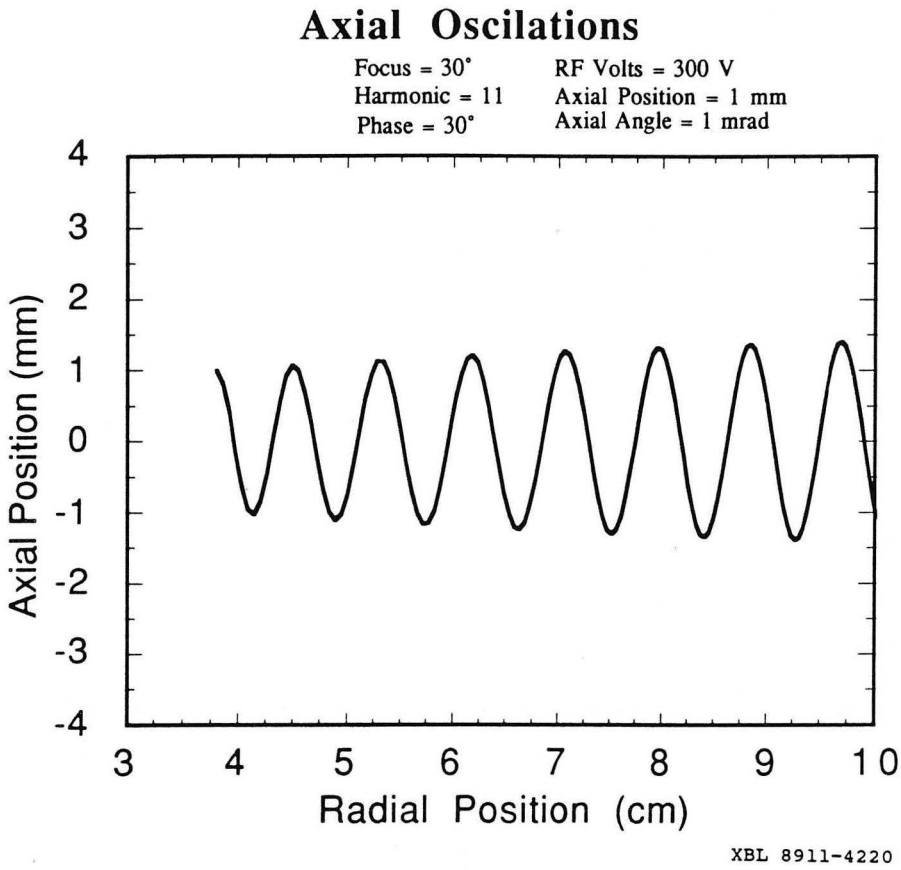
Axial Oscilations
Focus = 30°
Harmonic = 11
Phase = 30°
RF Volts = 300 V
Axial Position = 1 mm
Axial Angle = 1 mrad
Axial Position (mm)
4
3
2
1
0
-1
-2
-3
-4
3
4
5
6
7
8
9
10
Radial Position (cm)
XBL 8911-4220

Figure 5

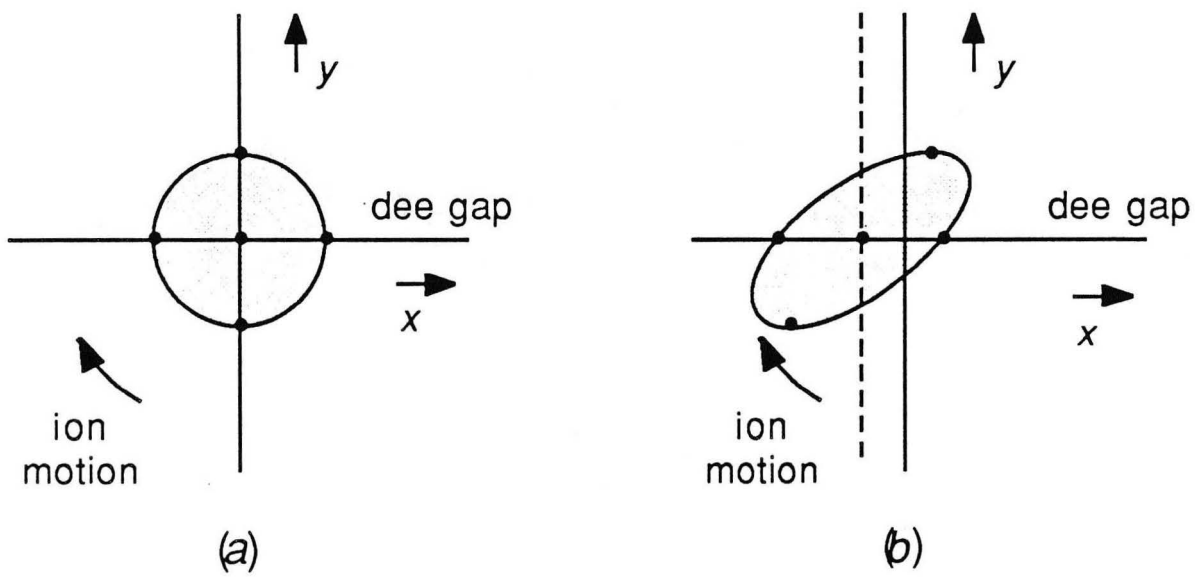

XBL 8911-4172

Figure 6

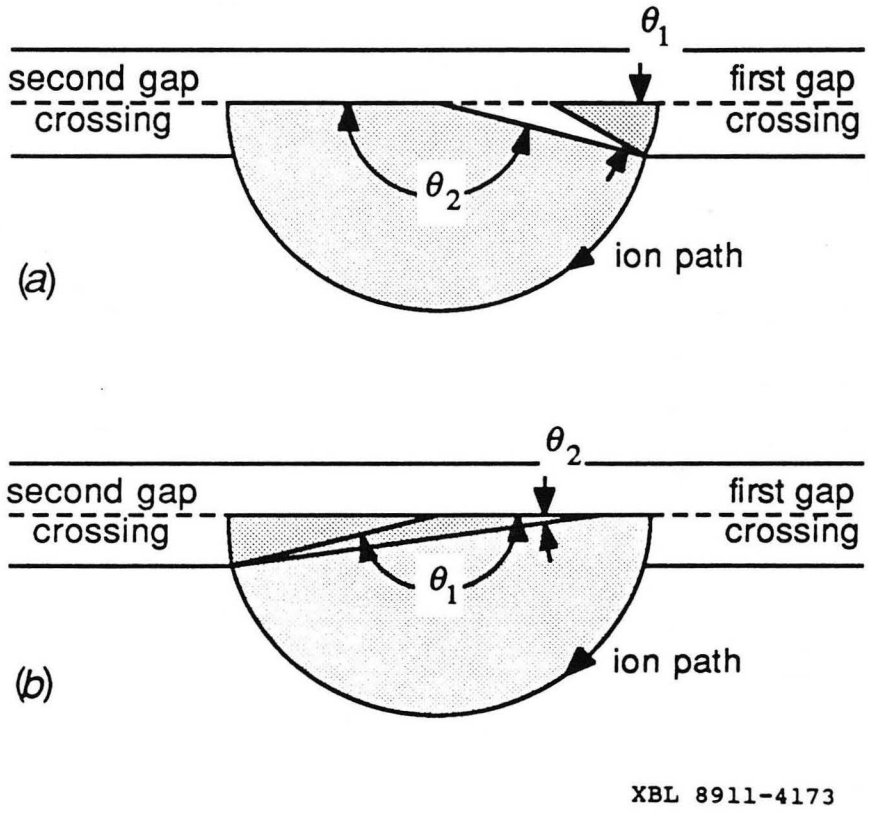
θ_1
second gap
crossing
first gap
crossing
θ_2
ion path
(a)
θ_2
second gap
crossing
first gap
crossing
θ_1
ion path
(b)
XBL 8911-4173

Figure 7

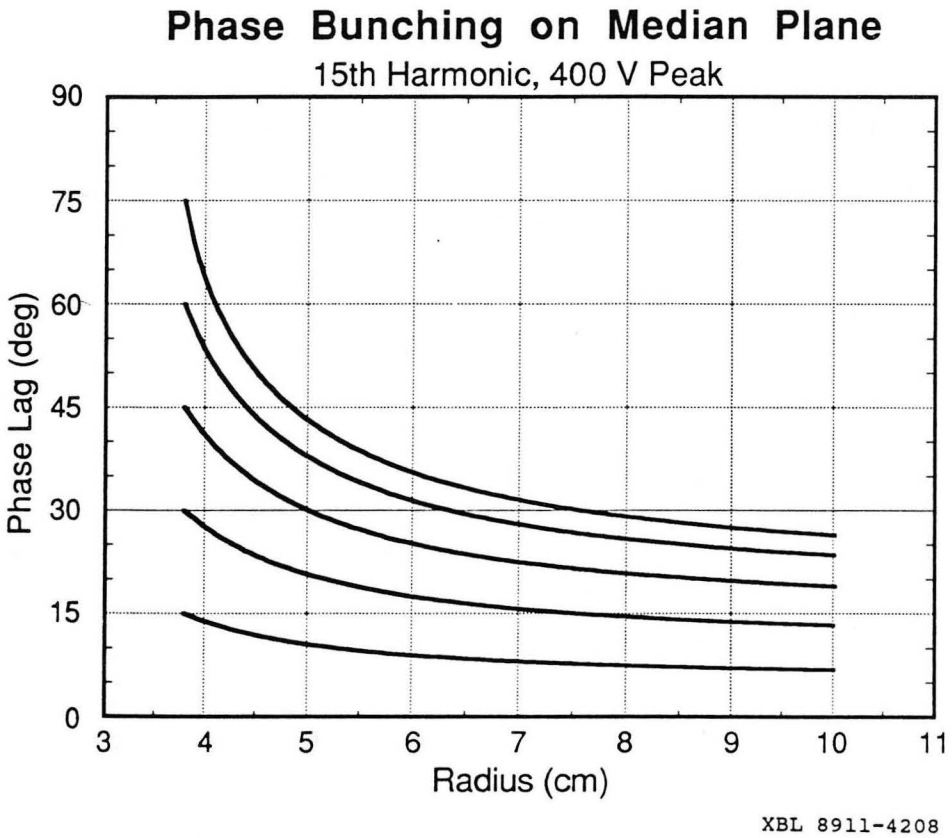
Phase Bunching on Median Plane
15th Harmonic, 400 V Peak
Phase Lag (deg)
90
75
60
45
30
15
0
3
4
5
6
7
8
9
10
11
Radius (cm)
XBL 8911-4208

Figure 8a

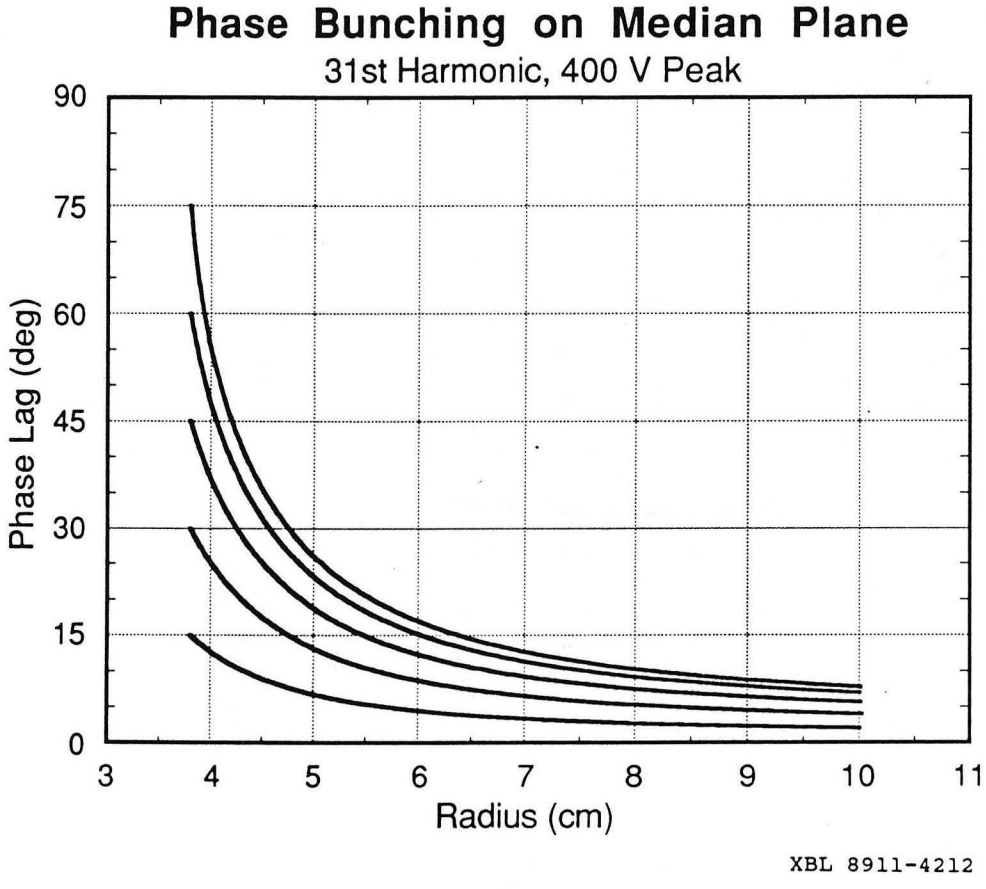
Phase Bunching on Median Plane
31st Harmonic, 400 V Peak
Phase Lag (deg)
90
75
60
45
30
15
0
3
4
5
6
7
8
9
10
11
Radius (cm)
XBL 8911-4212

Figure 8b

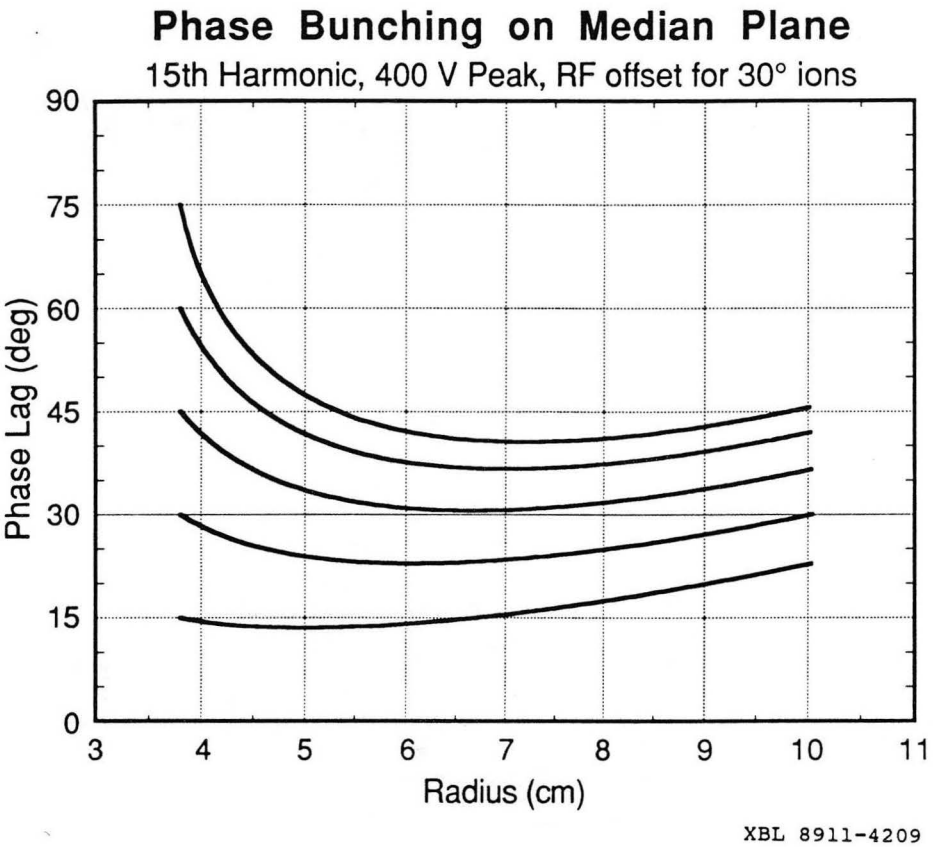
Phase Bunching on Median Plane
15th Harmonic, 400 V Peak, RF offset for 30° ions
Phase Lag (deg)
90
75
60
45
30
15
0
3
4
5
6
7
8
9
10
11
Radius (cm)
XBL 8911-4209

Figure 8c

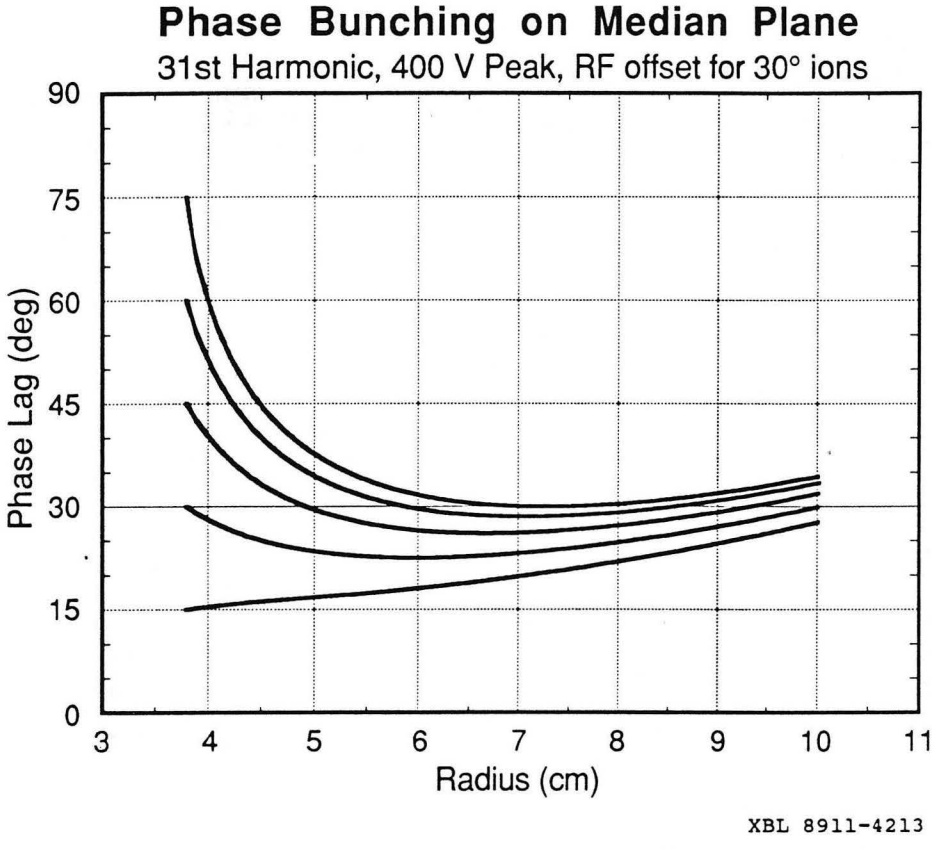
Phase Bunching on Median Plane
31st Harmonic, 400 V Peak, RF offset for 30° ions
Phase Lag (deg)
90
75
60
45
30
15
0
3
4
5
6
7
8
9
10
11
Radius (cm)
XBL 8911-4213

Figure 8d

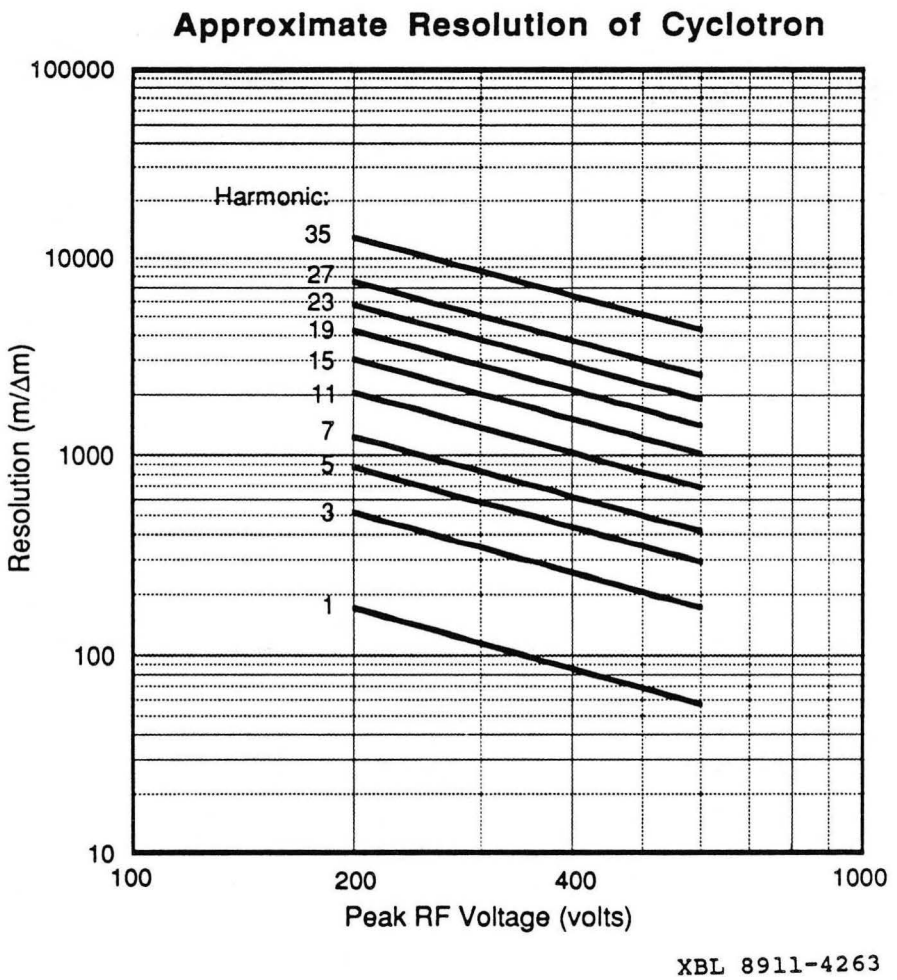
Approximate Resolution of Cyclotron
100000
10000
1000
100
10
Resolution (m/Δm)
Harmonic:
35
27
23
19
15
11
7
5
3
1
100
200
400
1000
Peak RF Voltage (volts)
XBL 8911-4263

Figure 9

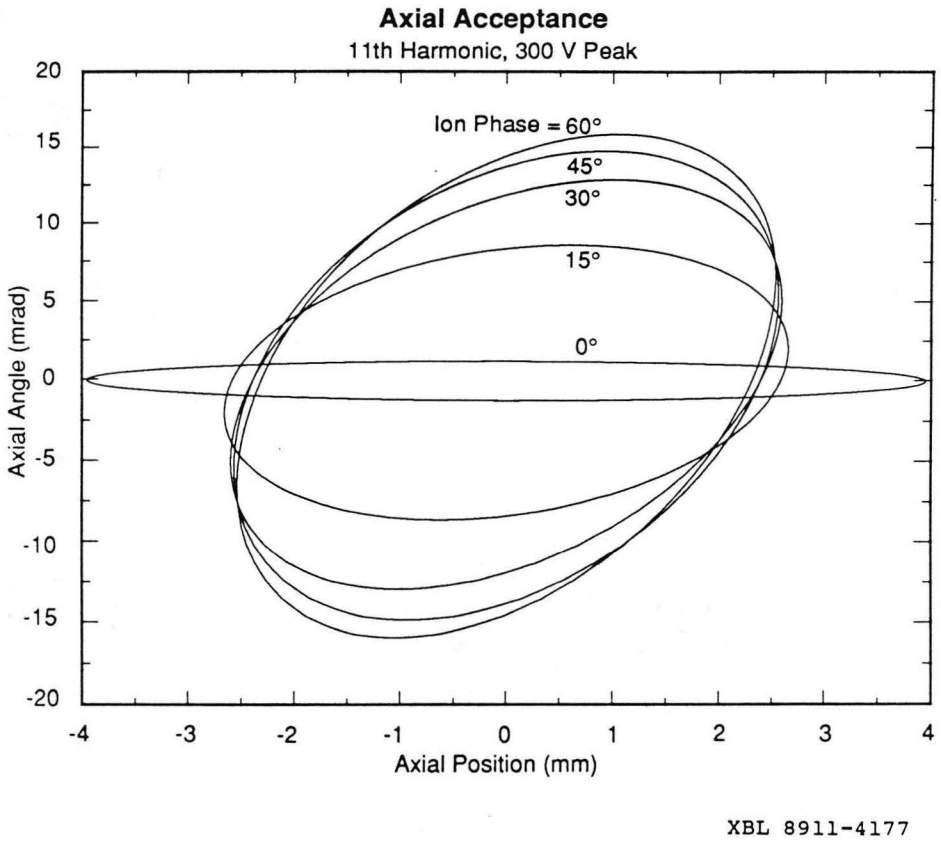
Axial Acceptance
11th Harmonic, 300 V Peak
Ion Phase = 60°
45°
30°
15°
0°
Axial Angle (mrad)
Axial Position (mm)
20
15
10
5
0
-5
-10
-15
-20
-4
-3
-2
-1
0
1
2
3
4
XBL 8911-4177

Figure 10a

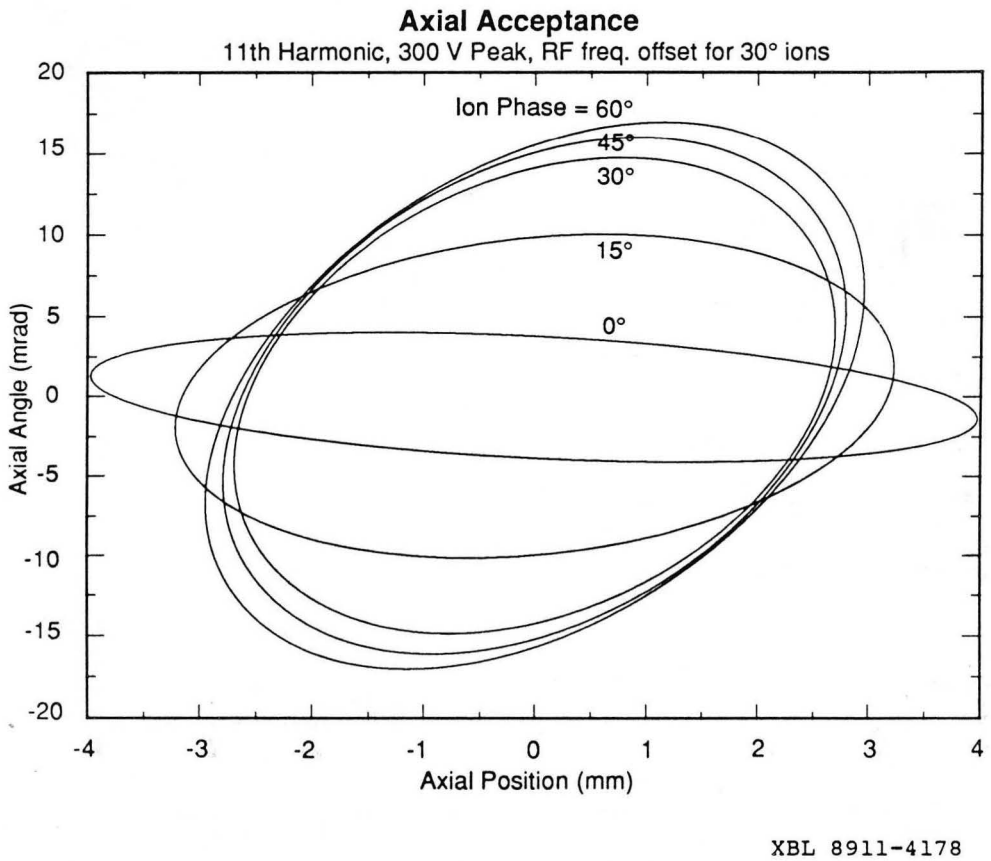
Axial Acceptance
11th Harmonic, 300 V Peak, RF freq. offset for 30° ions
Ion Phase = 60°
45°
30°
15°
0°
Axial Angle (mrad)
Axial Position (mm)
20
15
10
5
0
-5
-10
-15
-20
-4
-3
-2
-1
0
1
2
3
4
XBL 8911-4178

Figure 10b

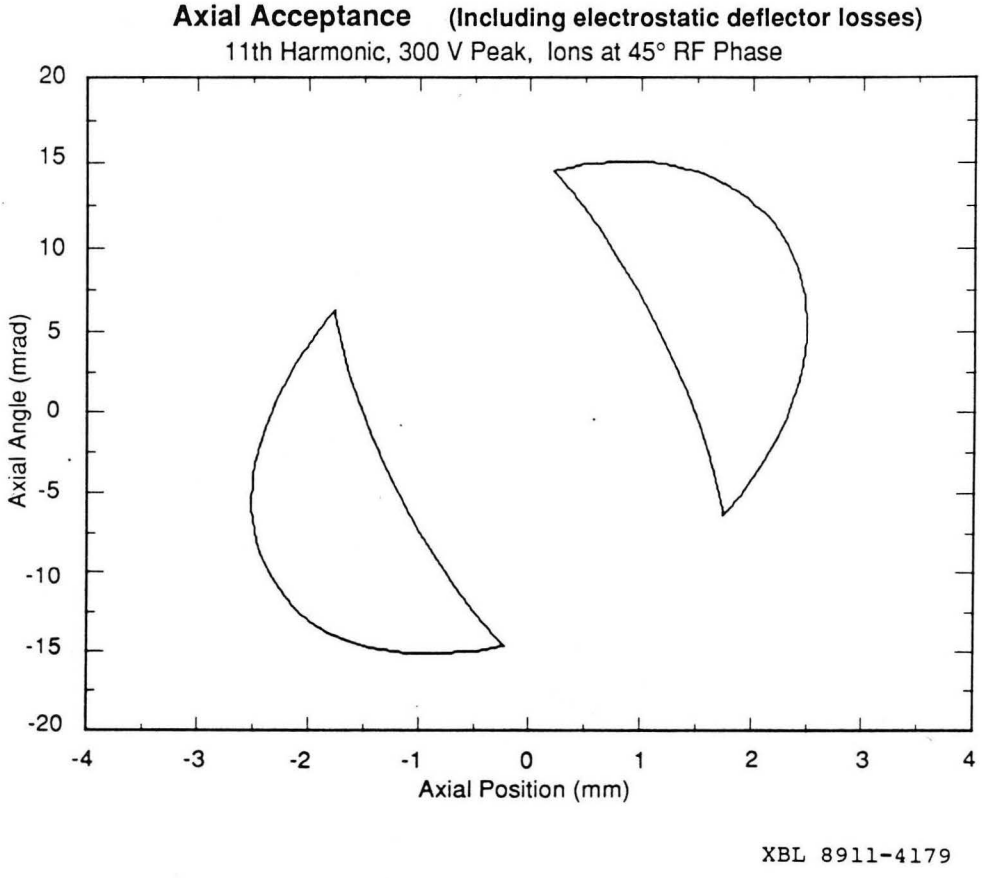
Axial Acceptance (Including electrostatic deflector losses)
11th Harmonic, 300 V Peak, Ions at 45° RF Phase
Axial Angle (mrad)
20
15
10
5
0
-5
-10
-15
-20
-4
-3
-2
-1
0
1
2
3
4
Axial Position (mm)
XBL 8911-4179

Figure 10c

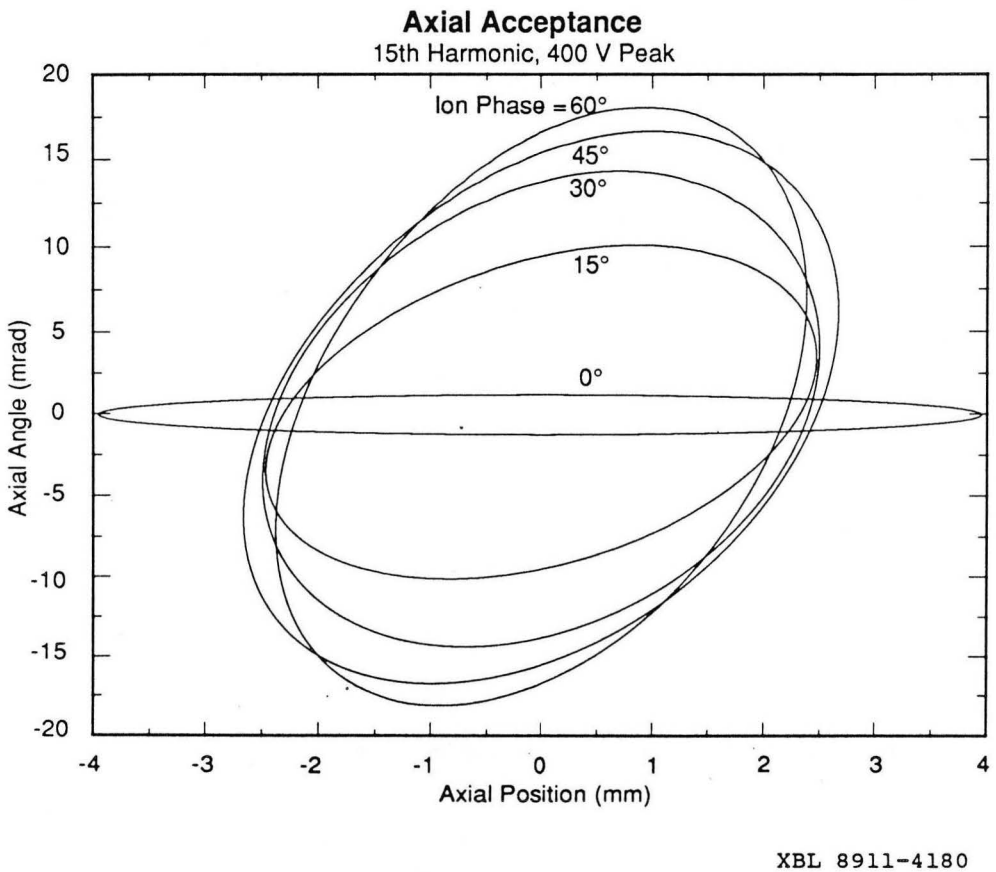
Axial Acceptance
15th Harmonic, 400 V Peak
Ion Phase = 60°
45°
30°
15°
0°
Axial Angle (mrad)
Axial Position (mm)
20
15
10
5
0
-5
-10
-15
-20
-4
-3
-2
-1
0
1
2
3
4
XBL 8911-4180

Figure 10d

LAWRENCE BERKELEY LABORATORY
UNIVERSITY OF CALIFORNIA
INFORMATION RESOURCES DEPARTMENT
BERKELEY, CALIFORNIA 94720